

Ti doped hematite thin film photoanode with enhanced photoelectrochemical properties

Xiaojuan Lian¹ · Jiang Cheng¹ · Rong Hu¹ · Hongdong Liu¹ · Xiaoqing Liao¹ · Lu Li¹ · Xin Yang¹

Received: 30 October 2015 / Accepted: 29 April 2016 / Published online: 3 May 2016
© Springer Science+Business Media New York 2016

Abstract Ti-doped Fe₂O₃ thin films were prepared on fluorine-doped SnO₂ substrate as visible light active photoelectrochemical anodes. The fabricated films were characterized by X-ray diffraction (XRD), scanning electron microscope (SEM), atomic force microscope (AFM), X-ray energy dispersive spectroscopy and X-ray photoelectron spectroscopy (XPS). XRD data showed all films exhibited rhombohedral hematite phase, and the cell parameters showed that Titanium atoms substituted Fe atoms in the hematite lattice. AFM demonstrated that Ti doping could decrease the particle size on the surface compared with pure hematite. XPS results presented that Ti atom concentration was about 2.23 % in the doped film surface. The incident photon to electron conversion efficiency of Ti doped α -Fe₂O₃ film reached 23 % at 400 nm under 0.30 V bias versus AgCl in 1 M NaOH, which was nearly four times than that of undoped film. Titanium atoms in α -Fe₂O₃ lattice could increase the conductivity of hematite film. And excited electrons and holes in the bulk film could be separated more efficiently, rather than recombining with each other rapidly as that in pure hematite, which ultimately prolonged the life of electrons and holes and obtained the high efficiency Fe₂O₃ photo anode.

1 Introduction

H₂ is clean, sustainable and vast storage energy on the earth; however, how to produce H₂ without exhausting other un-renewable energy is the key point. Solar energy may be the most probable source for H₂ production. After Honda and Fujishima first discovered n-type TiO₂ electrode can split water into H₂ and O₂ under irradiated sunlight [1]. Accordingly, hematite, with E_g = 2.0–2.2 eV, attribute to its stable, cheap and vast storage, became an ideal candidate for solar water splitting. For decades, a number of researches had been done on α -Fe₂O₃, and many methods were used for α -Fe₂O₃ preparation. Hardee etc. investigated the photo electrochemical performance of Fe₂O₃ pellets in the 1970s and find out that this material had a bad charge transport property, but the pellets still exhibited a good photo current [2]. Khan et al. [3] first calculated the total photo conversion efficiency of the α -Fe₂O₃ thin film photo anode, and the IPCE of the α -Fe₂O₃ anode prepared by USP method reached 5 % when tested in 1 M NaOH with a bias of 0.6 V versus SCE. Intrinsic α -Fe₂O₃ is an indirect semiconductor, and can hardly use most visible light. As a result, elements doping, such as Ti [4–6], Sn [7–9], etc. is one of the most effective way to obtain high photo electro chemical performance α -Fe₂O₃ thin film anode. Duret et al. [10] reported a large increase of IPCE value of hematite thin film prepared by APCVD with Si as doping material, and the IPCE reached 35 % at 400 nm with a bias of 1.23 V versus NHE. Glasscock et al. [11] characterized hematite thin film fabricated by reactive magnetron sputtering, and the IPCE was 15 % at 400 nm with a 1.23 V bias when doped with titanium. Nathan etc. reported hematite thin films prepared by reactive ballistic deposition method, which showed an IPCE of 13 % at 400 nm, and when doped with Ti and Sn, the IPCE increased to 23 and 18 % respectively [12]. Fu et al.

✉ Xin Yang
yangx@cqwu.edu.cn

¹ Co-innovation Center for Micro/Nano Optoelectronic Materials and Devices and Research Institute for New Materials Technology, Chongqing University of Arts and Sciences, Chongqing 402160, China

[6] reported that Ti-doped α - Fe_2O_3 with Al^{3+} treatment showed a 100 mV cathodic shift of the onset potential and a notable improvement of the photocurrent density, due to the surface states passivation.

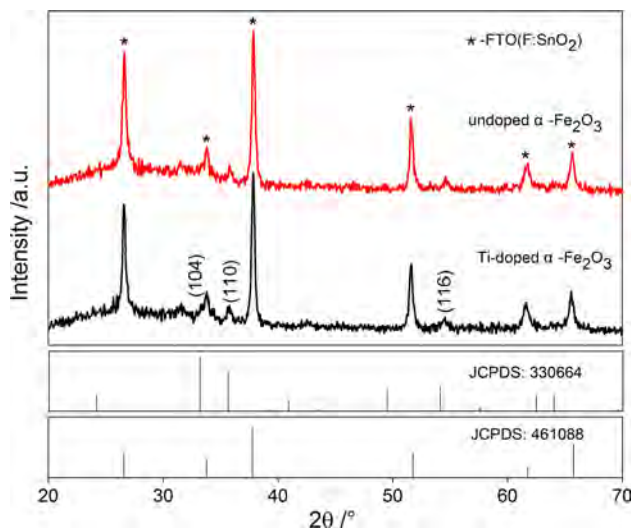


Fig. 1 XRD patterns of Ti-doped hematite and undoped hematite films on FTO substrates annealed in air for 2 h at 500 °C, the pentagrams denote peaks from FTO substrates

Magnetron sputtering is an ideal method for film deposition, which is well reproduction and easy for large scale fabrication. Here, hematite film anode was prepared with certain thickness to insure all PEC measurements were conducted under the same conditions.

2 Experiment

The fluorine doped SnO_2 glass (FTO, $14 \Omega/\square$, Pilkington) was cut into $2 \text{ cm} \times 2 \text{ cm}$ pieces. The glass was ultrasonicated in the NaOH and H_2O_2 mixed aqueous, acetone and ethanol ($\geq 30.0 \%$, Kelong Chemical) for 20 min, respectively. And then FTO was flushed by deionized water, dried by high pressure N_2 (99.99 %, Ruixin Gas). Pure and 5 atom % Ti-doped iron plate were used as sputtering targets. The metal film was deposited by JCP-350 magnetron sputtering system (Technol Science Co., Ltd) onto FTO glass with one edge sealed by polyimide tape for later photoelectrochemical test. The sputtering system worked under Ar (99.99 %, Ruixin Gas) atmosphere with a start vacuum of $5 \times 10^{-4} \text{ Pa}$. Then the sputtered Fe films were annealed at 500 °C for 2 h in a tube furnace at atmosphere.

The phase structure of films were characterized by X-Ray Diffraction (TD-3500X, Tongda instruments) with $\text{Cu K}\alpha_2$

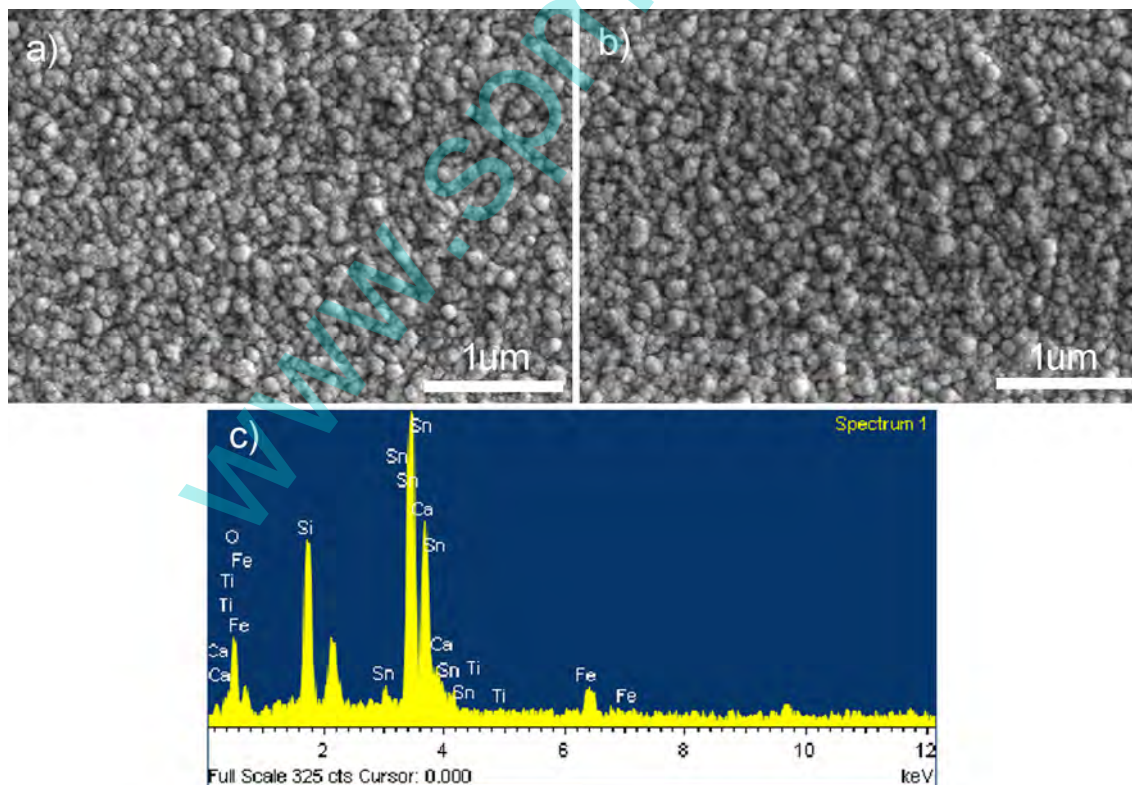


Fig. 2 SEM images of **a** undoped, **b** Ti-doped α - Fe_2O_3 and **c** EDS of Ti-doped α - Fe_2O_3 prepared by the thermal oxidizing method annealed at 500 °C

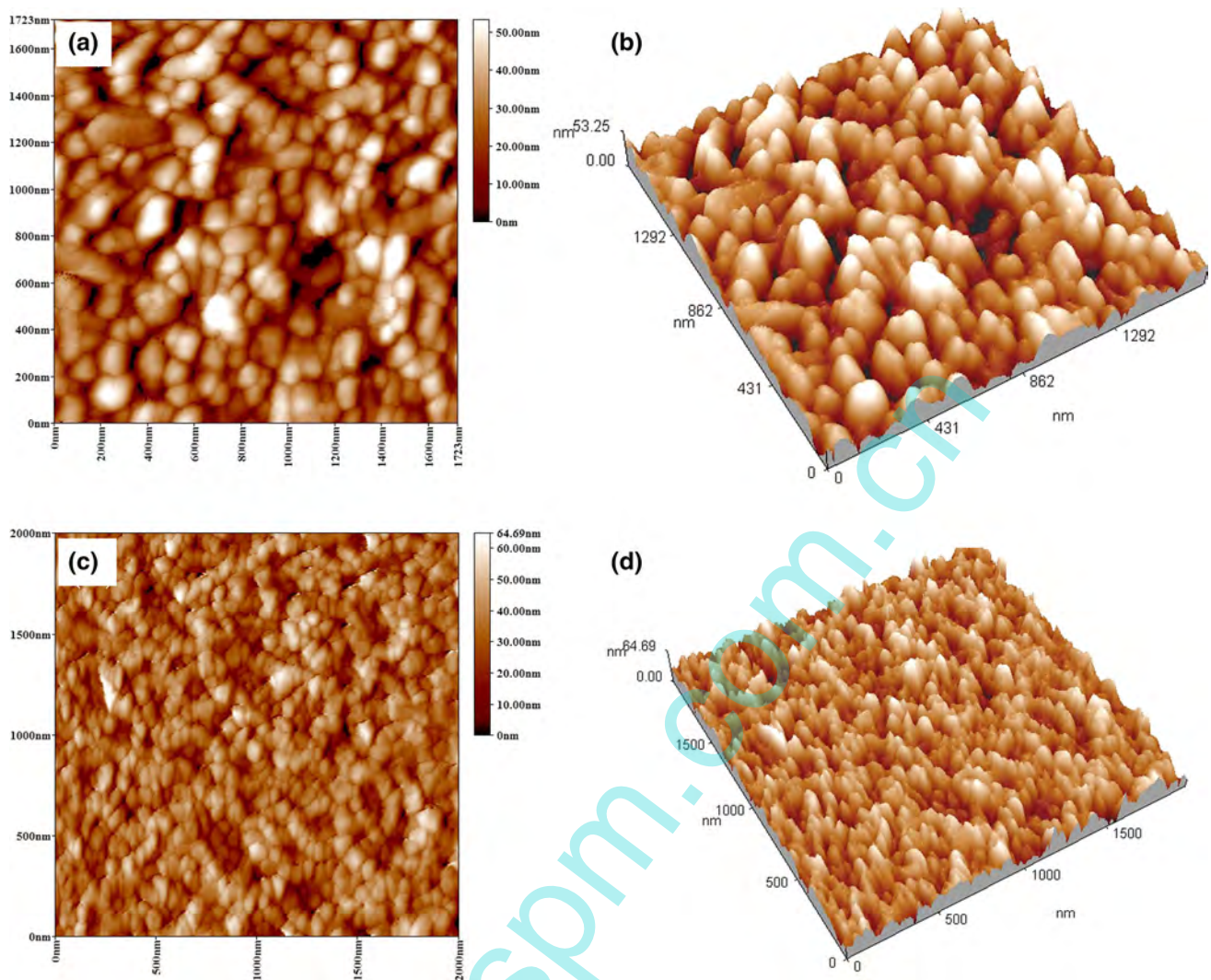


Fig. 3 AFM images of undoped and Ti-doped α -Fe₂O₃ prepared by the thermal oxidizing method annealed at 500 °C: **a** top morphology and **b** 3D image of undoped α -Fe₂O₃; **c** top morphology and **d** 3D image of Ti-doped α -Fe₂O₃

irradiation ($\lambda = 1.54056 \text{ \AA}$). The scan data were collected from 20° to 70° (2θ). The film morphology and EDS were analyzed by scanning electron microscope (SEM, S-4800, Hitachi) and atomic force microscope (AFM, CSPM4000, Benyuan). Film thickness was measured with D-100 style profiler (KLA Tencor, Ltd). UV–Vis absorption spectra were measured using UV–visible spectrophotometer (UV-3900, Hitachi). The blank FTO glass was used as the standard baseline. Photoelectrochemical performances were surveyed in a self-made three electrodes system in which a 1.0 mm thick quartz window was fitted to minimize light absorption, and make sure the electrode surface could facilitate the incidence of light as much as possible. Incident photo to electron conversion efficiency (IPCE) values of films were measured with PEC testing system (7-z, Ltd) calibrated by a single crystal Si solar cell.

3 Results and discussions

3.1 X-ray diffraction

Figure 1 shows the XRD patterns of undoped and Ti-doped film samples. Both of pure and Ti-doped Fe₂O₃ prepared after thermal annealing matched with the JC-PDS card no. 33-0664, corresponding to rhombohedral hematite. It was reported that Ti doping could affect the orientation of Fe₂O₃ lattice, when prepared by sol–gel spin-coating method [13]. However, no obvious preferential orientation occurred in (110) direction in our experiment. In addition, there was no phase data of TiO₂ detected in Ti doped hematite. As a result, we assumed that Ti atoms might substitute Fe atoms in the hematite lattice with only a small portion, leading to hardly any peak shifting of Ti doped

Table 1 (a) Elements, area (CPS), sensitivity factor and atomic surface proportion of detected elements for the Ti-doped hematite catalyst

| (a) Element | Area (CPS) | Sensitivity factor | Percentage | |
|-----------------|---------------|--------------------|------------|--------|
| Fe | 38,696.9 | 2 | 31.98 | |
| Ti | 1619.0 | 1.2 | 2.23 | |
| O | 26,270.7 | 0.66 | 65.79 | |
| (b) Peak (Fe2p) | Position (eV) | Area (CPS) | FWHM (eV) | GL (%) |
| 0 | 710.78 | 29,445.78 | 4.02 | 80 |
| 1 | 724.16 | 17,163.03 | 4.98 | 80 |
| 2 | 718.25 | 9251.08 | 4.06 | 80 |
| (c) Peak (Ti2p) | Position (eV) | Area | FWHM (eV) | GL (%) |
| 0 | 458.60 | 1619.02 | 2.18 | 80 |
| 1 | 463.65 | 1065.28 | 3.25 | 80 |

(b) Binding energy, area, FWHM and %GL of Fe2p. (c) Binding energy, area, FWHM and %GL of Ti 2p

hematite film or beyond the resolution of our XRD instrument to find out the peak shift. If Fe atom was replaced by Ti atom, each titanium atom could donor one free electron in the lattice, which could increase the conductivity of α -Fe₂O₃ thin film. The mean crystallite size are calculated from Debye–Scherrer's formula: $D = K\lambda/(\beta \cos \theta)$. Here D is the crystallite mean dimension, K is the Scherrer constant (K = 0.94), λ is the wavelength of Cu K α_1 , β is the full width at half maximum and θ is the Bragg diffraction angle. The calculation is based on the (104) peak. The grain size was 43 and 32 nm for pure hematite and Ti doped hematite film, respectively, which implied that Ti atoms in the hematite lattice might

introduce higher the boundary barrier and prevent the grain from growing.

3.2 SEM and AFM analysis

Figure 2 shows SEM images of α -Fe₂O₃ thin films, which are mainly composed of round particles. The particle size of the pure and Ti-doped hematite film was in the range of 40–100 nm, in accordance with Ti-doped hematite thin films prepared by magnetron sputtering [11]. Unlike the reported mesoporous hematite photoelectrodes prepared by solution-based methods [14, 15], the direct oxidized α -Fe₂O₃ exhibited dense surface. This difference might be caused by the preparation method and annealing process. Because most solution method employed Fe salts or other organic reagents, which decomposed during the annealing process and formed mesoporous or nanoporous film surface. AFM images showed that pure hematite film possesses smaller surface roughness than that of Ti-doped hematite film (Fig. 3). And the particle size of pure hematite film (80–150 nm) was bigger than that of Ti-doped hematite film (40–150 nm), due to the larger grain boundary barrier in the Ti doped film. However, during photoelectrochemical reaction, small surface particle size could provide larger contact area with electrolyte, which favored the charge separation process. The later PEC performance test would verify this hypothesis.

3.3 Photoelectron spectra analysis

Table 1 presents Elements, area (CPS), sensitivity factor and surface atomic proportion of detected elements for the Ti-doped hematite catalyst; Binding energy, area, FWHM and %GL of Fe 2p and Ti 2p orbitals. The calculated Fe, Ti

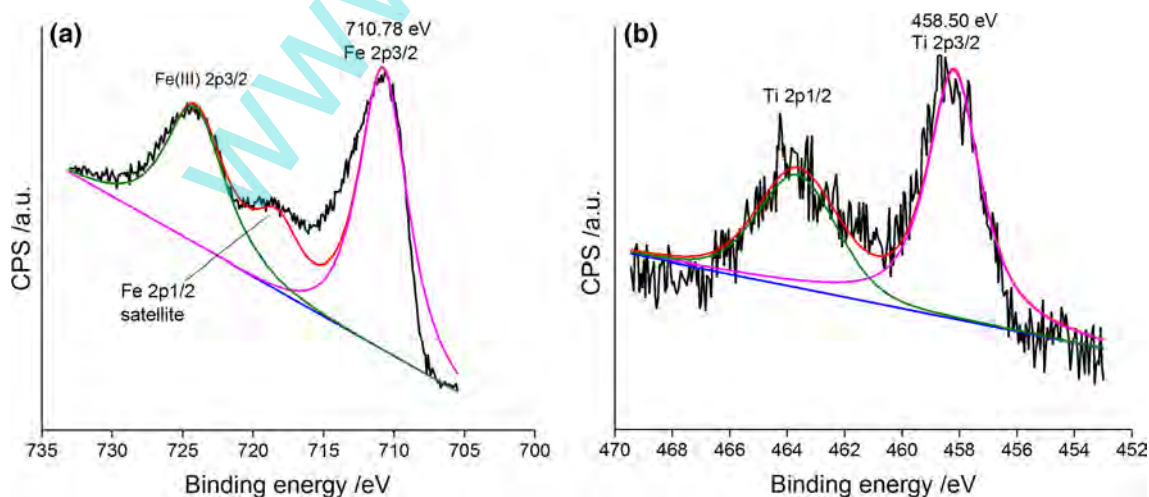


Fig. 4 XPS of **a** Fe 2p and **b** Ti 2p high-resolution spectra for the Ti-doped hematite thin film annealed in air for 2 h at 500 °C

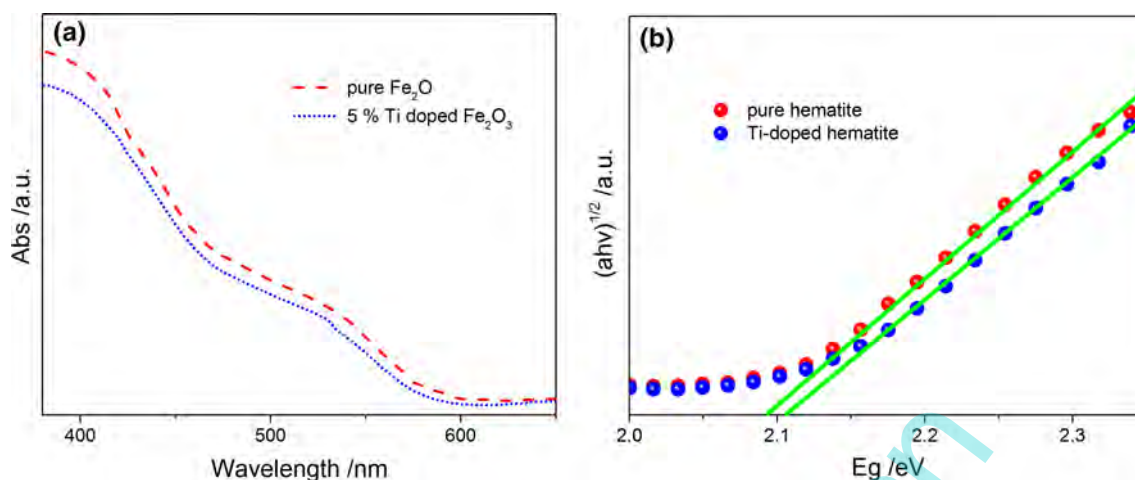


Fig. 5 **a** UV–visible absorbance spectra and **b** indirect band transition fit of undoped and Ti-doped hematite films

and O atomic percentages using area divided by sensitivity factor were around 31.98, 2.23 and 65.79 %, respectively. Figure 4 shows the X-ray photoelectron spectroscopy (XPS) spectrum of the core level Fe 2*p* in the Ti doped Fe₂O₃ thin film. The Fe 2*p*_{3/2} and Ti 2*p*_{3/2} peaks were located at 710.78 and 458.50 eV, which proved the presence of α-Fe₂O₃ and TiO₂ from the Ti-doped thin film, referring to the table of element electron binding energy [16, 17]. The B.E. of Ti 2*p*_{3/2} was 458.50 eV, while the standard B.E. of TiO₂ was about 458.7 eV. As a result, titanium existed in the form of TiO₂ in the Ti-doped α-Fe₂O₃ thin film, and the deviation of binding energy data might be caused by the mutual chemical reaction between Fe₂O₃ and TiO₂ [18–20]. In addition, X-ray energy dispersive spectroscopy (EDS) was used to determine the content of titanium. The result revealed that the mole percent of Ti was 5.6 %. The result is in good agreement with XPS test.

3.4 UV–Vis absorbance spectrum

The undoped and Ti-doped hematite films were semi-transparent orange-brown. UV–visible absorbance spectra of each sample were shown in Fig. 5a. The thickness was 97 and 100 nm for pure and Ti-doped hematite films respectively. The deduction of energy gap was based on Tauc formula [21]: $(\alpha h\nu)^n \propto A(h\nu - E_g)$. Here, α is the absorption coefficient, $n = 1/2$ for indirect transition and $n = 2$ for direct transition. A is the proportionality constant, $h\nu$ the photon energy and E_g the energy gap. Figure 5b shows that both films exhibit indirect transition gap from 590 to 460 nm, which has been identified as Fe³⁺ 3*d* → 3*d* excitation. However, when the wavelength decreased below 420 nm, the O²⁻ 2*p* → Fe³⁺ 3*d* transition became the main way and α-Fe₂O₃ exhibited direct

transition [10]. Instead of increasing, the absorbance of Ti doped film became smaller than the pure Fe₂O₃ film in the short wavelength scale. Since TiO₂ have a wide $E_g = 3.2$ eV, the optical band gap of Ti doped Fe₂O₃ film was a little wider than undoped hematite (Fig. 5b).

3.5 Incident photo to electron conversion efficiency

The photoelectrochemical performance is estimated by incident photo to electron conversion efficiency (IPCE), which is given by the formula: $IPCE = \frac{j}{P_{in}} \frac{1240}{\lambda} \times 100\%$. Here, j is the photocurrent density (mA cm⁻²), λ is the wavelength (nm) and P_{in} represents the power of monochromatic light irradiated on the electrode (mW cm⁻²).

Figure 6 shows the IPCE measurements were carried out under the bias of 0.3 V versus Ag/AgCl in 1 M NaOH

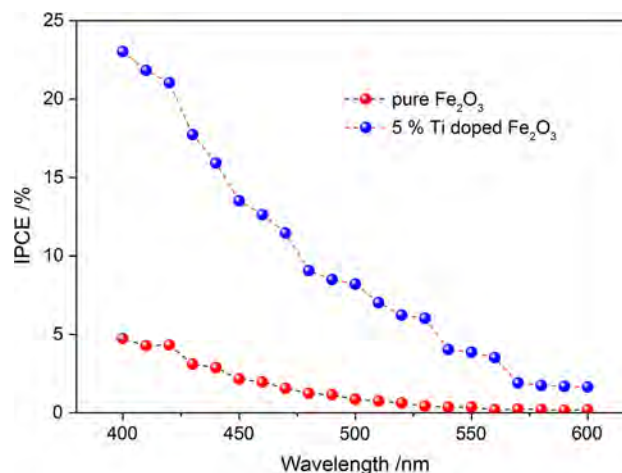


Fig. 6 IPCE performance of undoped and Ti-doped Fe₂O₃ thin films on FTO substrates annealed at 500 °C

solution. IPCE of Ti doped thin film (23 % at 400 nm) was nearly fourth times of undoped Fe_2O_3 thin film. Assume that Fe was substituted by Ti in the hematite lattice; Ti^{4+} played the role of electron donor and contributes one free electron in the hematite lattice. The bulk conductivity of the doped hematite could be improved than that of the undoped hematite by suppressing the charge recombination in the bulk film, because the hole diffusion length was only about 10 nm in $\alpha\text{-Fe}_2\text{O}_3$ [13]. Therefore when the amount of photo generated carriers were the same in both Ti-doped and pure hematite films, Ti-doped film could transfer electrons more efficiently and perform a better photo current during the test. From the XPS surface Ti atomic concentration, TiO_2 formed in the Fe_2O_3 surface, which could improve the electron transfer efficiency on the interface between Fe_2O_3 film and electrolyte.

4 Conclusions

The pure and Ti-doped Fe_2O_3 photo anodes were prepared on FTO substrates by magnetron sputtering. The photoelectrochemical properties were investigated in a three-electrode system. Due to the surface abundant of Ti^{4+} ion, the IPCE of Ti-doped hematite thin film was almost three times higher than that of undoped Fe_2O_3 at 400 nm. The highest IPCE could reach 23 % under 0.3 V versus Ag/AgCl. The possible explanation was that Ti^{4+} in the bulk film could improve the conductivity and TiO_2 on the film surface acting as excellent catalyst for charge transfer between film and electrolyte. Optimization of the Ti-doped Fe_2O_3 was still underway to improve the photoelectrochemical properties.

Acknowledgments This work was financially supported by NSFC (61505018), Chongqing Education government (KJ1401113, Ycstc2015nc4002), and Science Projects of Chongqing University of Arts and Sciences (R2013CJ08 and Y2015XC27).

References

1. A. Fujishima, *Nature* **238**, 37 (1972)
2. K.L. Hardee, A.J. Bard, *J. Electrochem. Soc.* **123**, 1024 (1976)
3. S.U.M. Khan, J. Akikusa, *J. Phys. Chem. B* **103**, 7184 (1999)
4. Z. Fu, T. Jiang, Z. Liu, D. Wang, L. Wang, T. Xie, *Electrochim. Acta* **129**, 358 (2014)
5. P. Zhang, A. Kleiman-Shwarscstein, Y.-S. Hu, J. Lefton, S. Sharma, A.J. Forman, E. McFarland, *Energ. Environ. Sci.* **4**, 1020 (2011)
6. Z. Fu, T. Jiang, L. Zhang, B. Liu, D. Wang, L. Wang, T. Xie, *J. Mater. Chem. A* **2**, 13705 (2014)
7. S. Park, H.J. Kim, C.W. Lee, H.J. Song, S.S. Shin, S.W. Seo, H.K. Park, S. Lee, D.-W. Kim, K.S. Hong, *Int. J. Hydrogen. Energ.* **39**, 16459 (2014)
8. H.K. Dunn, J.M. Feckl, A. Mueller, D. Fattakhova-Rohlfing, S.G. Morehead, J. Roos, L.M. Peter, C. Scheu, T. Bein, *Phys. Chem. Chem. Phys.* **16**, 24610 (2014)
9. Y. Ling, Y. Li, *Part. Part. Syst. Char.* **31**, 1113 (2014)
10. A. Duret, M. Grätzel, *J. Phys. Chem. B* **109**, 17184 (2005)
11. J.A. Glasscock, P.R.F. Barnes, I.C. Plumb, N. Savvides, *J. Phys. Chem. C* **111**, 16477 (2007)
12. N.T. Hahn, H. Ye, D.W. Flaherty, A.J. Bard, C.B. Mullins, *ACS Nano* **4**, 1977 (2010)
13. X. Lian, X. Yang, S. Liu, Y. Xu, C. Jiang, J. Chen, R. Wang, *Appl. Surf. Sci.* **258**, 2307 (2012)
14. J. Deng, J. Zhong, A. Pu, D. Zhang, M. Li, X. Sun, S.-T. Lee, *J. Appl. Phys.* **112**, 084312 (2012)
15. K. Sivula, R. Zboril, F. Le Formal, R. Robert, A. Weidenkaff, J. Tucek, J. Frydrych, M. Grätzel, *J. Am. Chem. Soc.* **132**, 7436 (2010)
16. M. Aronniemi, J. Lahtinen, P. Hautojärvi, *Surf. Interface Anal.* **36**, 1004 (2004)
17. D.W. Sheel, J. Lewis, A. Robinson, H.M. Yates, *ECS Trans.* **25**, 1081 (2009)
18. M.R. Dhananjeyan, E. Mielczarski, K.R. Thampi, P. Buffat, M. Bensimon, A. Kulik, J. Mielczarski, J. Kiwi, *J. Phys. Chem. B* **105**, 12046 (2001)
19. N. Hellgren, M.P. Johansson, E. Broitman, L. Hultman, J.-E. Sundgren, *Phys. Rev. B* **59**, 5162 (1999)
20. R. Lopez, R. Gomez, M.E. Llanos, *Catal. Today* **148**, 103 (2009)
21. J. Tauc, *Science* **158**, 1543 (1967)